

UC Santa Barbara

UC Santa Barbara Previously Published Works

Title

Structural and Spectroscopic Characterization of a Zinc-Bound N-Oxyphthalimide Radical

Permalink

<https://escholarship.org/uc/item/3cf9b5fm>

Journal

Inorganic Chemistry, 61(34)

ISSN

0020-1669

Authors

Cinco, Miguel A Baeza
Wu, Guang
Telser, Joshua
[et al.](#)

Publication Date

2022-08-29

DOI

10.1021/acs.inorgchem.2c01765

Copyright Information

This work is made available under the terms of a Creative Commons Attribution License, available at <https://creativecommons.org/licenses/by/4.0/>

Peer reviewed

Structural and Spectroscopic Characterization of a Zinc-bound *N*-oxyphthalimide Radical

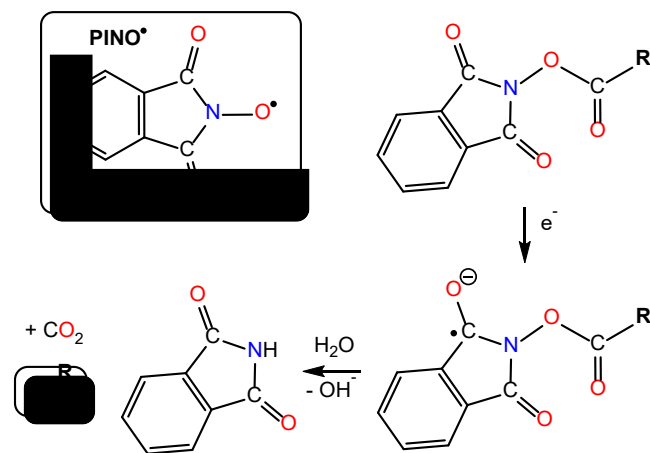
Miguel Á. Baeza Cinco,† Guang Wu,† Joshua Telser,‡ Trevor W. Hayton†*

†Department of Chemistry and Biochemistry, University of California, Santa Barbara, Santa Barbara, CA 93016 (USA)

‡Department of Biological, Chemical and Physical Sciences, Roosevelt University, 430 S. Michigan Ave. Chicago, Illinois 60605-1394 United States.

ABSTRACT: Thermolysis of a 1:1:1 mixture of ^{Me}LH (^{Me}L = {(2,6-ⁱPr₂C₆H₃)NC(Me)₂CH}, *N*-hydroxyphthalimide (HOPth), and ZnEt₂ in toluene at 77 °C provided [^{Me}LZn(OPth)] (**1**) in good yield after work-up. Subsequent reduction of **1** with 1.3 equiv of K⁺C₈ and 1 equiv of 2.2.2-cryptand, in THF, provided [K(2.2.2-cryptand)][^{Me}LZn(OPth)] (**2**) in 74 % yield after work-up. Characterization of **2** via X-ray crystallography and EPR spectroscopy reveals the presence of an *S* = 1/2 radical on the *N*-oxyphthalimide ligand. Importantly, these data represent the first structural and spectroscopic confirmation of the redox activity of a metal-bound *N*-oxyphthalimide fragment, expanding the range of structurally characterized redox-active ligands.

The utility of *N*-hydroxyphthalimide (HOPth) and its derivatives in synthetic chemistry has been well established over the past two decades.¹⁻⁵ For example, the highly reactive phthalimide *N*-oxyl radical (i.e., PINO[•]; Scheme 1, inset), which is generated from HOPth *in situ*, can oxidize a variety of organic substrates, including lignin model compounds,⁶ cycloalkanes,⁷⁻¹¹ alkenes,¹²⁻¹⁵ and alcohols,¹⁶⁻¹⁹ as well as a wide variety of benzylic compounds,²⁰⁻²⁶ under both metal-free and metal-assisted conditions. *N*-(acyloxy)phthalimides and *N*-alkoxyphthalimides have also found widespread use, specifically as convenient sources of alkyl radicals.^{5, 27} This approach was pioneered by Okada and co-workers, who demonstrated that *N*-(acyloxy)phthalimides could cross-couple with electron-deficient olefins under photocatalytic conditions.^{28, 29} The proposed mechanism involves a photo-initiated reduction of the *N*-(acyloxy)phthalimide to form a radical anion, which subsequently undergoes decarboxylation and formation of an alkyl radical (Scheme 1), which is then trapped by substrate.



Scheme 1. Proposed mechanism of alkyl radical generation from *N*-(acyloxy)phthalimide. Inset: molecular structure of phthalimide *N*-oxyl radical (PINO[•]).

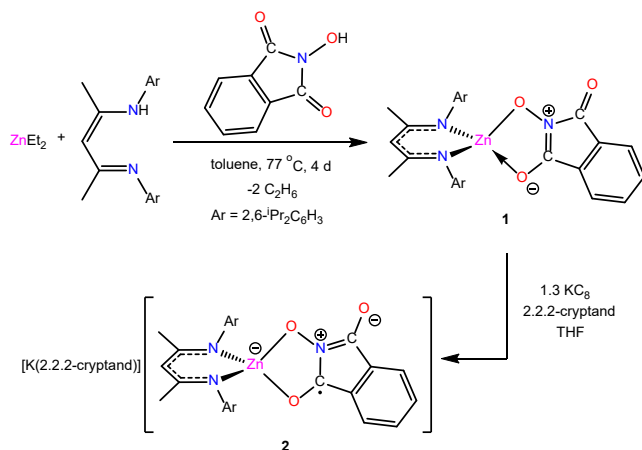
This method of alkyl radical generation has since been widely adopted,^{5, 30} and includes examples of its use in alkylation,³¹⁻³³ aminylation,^{34, 35} alkoxylation,³⁶ borylation,^{37, 38} indenylation,³⁹ arylation,⁴⁰ and alkenylation.^{30, 41, 42} This methodology has also been incorporated into the synthesis of complex natural products.⁴³⁻⁴⁵ These transformations are often metal-catalyzed, and while the proposed catalytic cycles do not typically invoke L_nM(OPth) complex formation, it seems reasonable that electron transfer to the phthalimide group could occur via an inner sphere mechanism. However, our structural understanding of metal *N*-oxyphthalimide complexes is limited. Indeed, only a handful have been structurally characterized, including [(*n*-Bu₃P)Ag(OPth)]₂,⁴⁶ [Cr(N)(OPth)(NⁱPr₂)₂],⁴⁷ and [Sb(OPth)₂Ph₃].⁴⁸ More importantly, to our knowledge, there are no reported structurally characterized examples of the OPth radical species, which hampers our understanding of the mechanism of decarboxylation and potentially limits the further development of this chemistry.

Nonetheless, our general understanding of redox non-innocent ligands has grown significantly in recent years.⁴⁹⁻⁵⁶ Complexes with redox non-innocent ligands have proven useful in catalysis, where the non-innocent ligands function as electron reservoirs, allowing first row transition metals to easily perform multi-electron transformations.⁵⁷ Redox non-innocent ligands can also enable multi-electron chemistry in the actinides,⁵⁸⁻⁶⁰ and they play an important role in biology.⁶¹

Previously, we reported on the synthesis and reactivity of a series of metal complexes containing the redox-active TEMPO ligand, including [FeCl₃(η¹-TEMPO)] (TEMPO = 2,2,6,6-tetramethylpiperidine-*N*-oxide), [AlX₃(η¹-TEMPO)] (X = Cl, Br), and [(η¹-TEMPO)₂BBr].⁶²⁻⁶⁴ In these examples, the TEMPO moiety was bound to the metal ion in both its radical and anionic forms. Building on this work, we have

now prepared a novel β -diketiminato-supported⁶⁵ Zn phthalimide *N*-oxide complex, which allowed us to explore the redox activity of the phthalimide fragment, using both structural and spectroscopic techniques.

Heating a 1:1:1 mixture of MeLH ($\text{MeL} = \{(2,6\text{-}i\text{Pr}_2\text{C}_6\text{H}_3)\text{NC}(\text{Me})_2\text{CH}\}$), HOPth, and ZnEt_2 in toluene at 77 °C for 4 d produced a bright orange suspension. Work-up of this reaction mixture provided $[\text{MeLZn}(\text{OPth})]$ (**1**) in 77% isolated yield (Scheme 2, top).



Scheme 2. Syntheses of complexes **1** and **2**.

Complex **1** crystallizes with two independent molecules in the asymmetric unit as the Et₂O solvate, **1**·1.5Et₂O. It features a tetrahedral Zn²⁺ center, wherein the OPth ligand adopts a bidentate *O,O*- κ^2 coordination mode (Figure 1; crystallographic data are given in the SI, Table S1). The metrical parameters of the two molecules within the asymmetric unit are very similar, and the parameters of only one will be discussed in detail. Not surprisingly, the Zn–O distance of the *N*-bound oxygen atom (Zn1–O2 = 1.979(2) Å; Figure 2) is shorter than the Zn–O distance of the *C*-bound oxygen atom (Zn1–O1 = 2.088(2) Å), reflecting the greater anionic character of O2. Additionally, the C–O distance of the Zn-bound carbonyl group is longer (C30–O1 = 1.246(3) Å) than the C–O distance of the free carbonyl (C31–O3 = 1.208(4) Å), consistent with activation of the C=O fragment upon ligation to Zn²⁺. The phthalimide N–C distances in **1** are also inequivalent (i.e., N3–C31 = 1.414(4) Å and N3–C30 = 1.353(3) Å). Overall, these metrical parameters suggest the presence of localized π -bonds between N3 and C30 and between O3 and C31, as drawn for **1** in Scheme 2. Consistent with this suggestion, the sum of interatomic angles around N3 is 359.9°, as expected for an sp²-hybridized nitrogen. For comparison, the C–O distances in free HOPth are equivalent (1.210(5) and 1.214(5) Å; Figure 2). The N–C distances in free HOPth are also equivalent (1.384(6) and 1.397(6) Å). Both observations are consistent with a delocalized electronic structure in HOPth, in contrast to the situation for **1**.

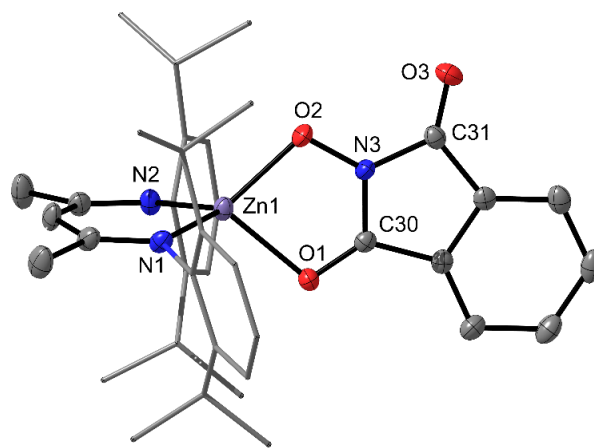


Figure 1. Solid-state structure of **1**·1.5Et₂O. Thermal ellipsoids set at 50% probability. Et₂O solvate molecules and hydrogen atoms omitted for clarity. *N*-aryl substituents shown in wireframe.

To our knowledge, the *O,O*- κ^2 *N*-oxy-phthalimide binding mode observed in **1** is unique. For comparison, $[(n\text{-Bu}_3\text{P})\text{Ag}(\text{OPth})]_2$ and $[\text{Sn}_4\text{O}_2\text{Me}_8\text{Cl}_2(\text{OPth})_2]$ exhibit *O*- κ^1 : μ binding modes of their phthalimide ligands,^{46, 66} whereas $[\text{Cr}(\text{N})(\text{OPth})(\text{N}^i\text{Pr}_2)_2]$ and $[\text{Sb}(\text{OPth})_2\text{Ph}_3]$ exhibit *O*- κ^1 binding modes.^{47, 48} Interestingly, in these examples the *N*-oxy-phthalimide group maintains its delocalized electronic structure. For example, $[(n\text{-Bu}_3\text{P})\text{Ag}(\text{OPth})]_2$ exhibits indistinguishable N–C distances (1.389(1) and 1.397(1) Å) and indistinguishable C–O distances (1.219(1) and 1.213(1) Å).

The ¹H NMR spectrum of complex **1** in C₆D₆ features doublets at 6.77 and 6.47 ppm, which are assignable to the two unique C–H environments on the *N*-oxy-phthalimide ligand (Figure S1). Likewise, the spectrum features doublets at 1.53 and 1.20 ppm, which are assignable to the two diastereotopic isopropyl CH₃ environments of the *N*-aryl substituents of the β -diketiminato ligand. Both observations are diagnostic of a *C*_{2v}-symmetric complex, which contrasts with the *C*_s symmetry observed in the solid-state. This discrepancy can be rationalized by invoking rapid exchange of the Zn-ligated carbonyl group (O1 in Figure 1) with the unligated carbonyl group (O3). Alternatively, the OPth ligand may adopt an η^1 coordination mode in solution, as is observed for $[\text{Cr}(\text{N})(\text{OPth})(\text{N}^i\text{Pr}_2)_2]$ and $[\text{Sb}(\text{OPth})_2\text{Ph}_3]$.^{47, 48} The IR spectrum of **1** (KBr pellet) features ν_{CO} modes at 1793 and 1766 cm⁻¹ (Figure S9). For comparison, free HOPth features ν_{CO} modes at slightly higher energies (1833 and 1782 cm⁻¹), consistent with the weakening expected upon ligation.⁶⁷ Finally, the cyclic voltammogram of **1** in THF reveals a reversible oxidation feature at –1.84 V (vs Fc/Fc⁺; Figure S13), which we attribute to the reduction of the *N*-oxy-phthalimide ligand.

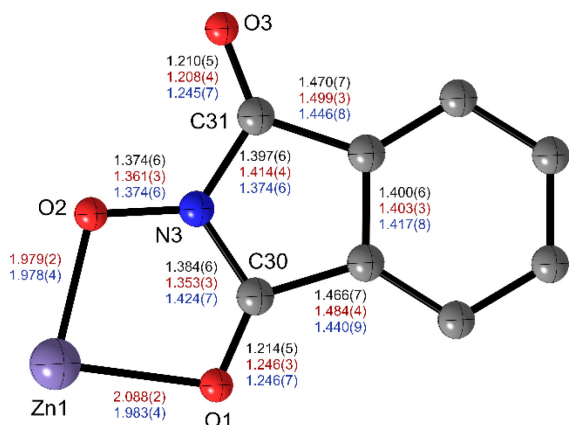


Figure 2. Bond distance (Å) comparison for free HOPth (black), **1**·1.5Et₂O (red), and **2** (blue). Carbon atoms shown in gray, oxygen atoms shown in red, nitrogen atom shown in blue, and zinc atom shown in lavender. Structure shown is that of **1**. Metrical parameters for HOPth taken from Ref 68.

The cyclic voltammogram of **1** suggested that its 1e⁻ reduction product could be isolable. Gratifyingly, reaction of **1** in THF with 1.3 equiv of K₂C₈, in the presence of 2.2.2-cryptand, quickly produced a deep olive green solution. Work-up of the reaction mixture permitted isolation of [K(2.2.2-cryptand)][^{Me}LZn(OPth)] (**2**) in 74% yield (Scheme 2, bottom). Consistent with the anticipated paramagnetism, the signals in its ¹H NMR spectrum are extremely broad (Figure S3). In particular, a broad resonance at 5.11 ppm is assignable to the γ-CH position of the β-diketiminato ligand, whereas broad resonances at 2.04 and 1.35 ppm are assignable to its diastereotopic isopropyl CH₃ groups of the *N*-aryl substituents. Additionally, we observe broad resonances at 3.17 and 2.23 ppm, which are assignable to the 2.2.2-cryptand moiety. Finally, the IR spectrum of **2** (KBr pellet) features a ~100 cm⁻¹ redshift of its ν_{CO} modes relative to **1** (Figure S10), consistent with the expected decrease in the C=O bond order upon reduction.

Complex **2** was also characterized by X-ray crystallography. It crystallizes in the triclinic space group *P*-1 as a discrete cation/anion pair (Figure S8). As was observed for **1**, its OPth ligand is bound in a *O,O*-κ² fashion to the tetrahedral Zn²⁺ center. Additionally, the Zn–O distance of the *N*-bound oxygen atom (Zn1–O2 = 1.978(4) Å; Figure 2) is indistinguishable to that observed for **1** by the 3σ criterion. In contrast, however, the Zn–O distance of the *C*-bound oxygen atom in **2** (1.983(4) Å) is considerably shorter (Figure 2). Moreover, the two C–O distances in **2** are within error (1.246(7) and 1.254(7) Å), while the N–C distances are inequivalent (1.424(7) and 1.374(6) Å). Overall, these metrical parameters suggest the presence of a localized π-bond between N3 and C31 and localization of the unpaired electron at C30, as drawn for **2** in Scheme 2. The sum of interatomic angles around N3 (360.0°) is also consistent with this hypothesis.

The X-band solution-phase EPR spectrum of complex **2**, recorded in toluene at room temperature, displays a narrow isotropic peak at *g* = 2.0010 indicative of an *S* = 1/2 organic radical (Figure 3; see also Figure S5).⁶⁹ Upon cooling to 110 K, the EPR spectrum of **2** remains centered at the same *g*

value, but broadens somewhat (Figure S6). To better understand these spectra, the electronic structure of **2** was investigated by density functional theory (DFT) calculations using the ORCA software package.^{70,71} For computational efficiency and simplicity, the β-diketiminato Ar groups were replaced by Me groups. This truncated structure is denoted **2'**. The [K(2.2.2-cryptand)]⁺ moiety was also omitted. Its optimized geometry, **2'-opt**, differs only slightly from the experimental structure (Figures S14 and S15; Cartesian coordinates are given in Table S4). Nevertheless, the optimized structure maintained the *O,O*-κ² chelate interaction.

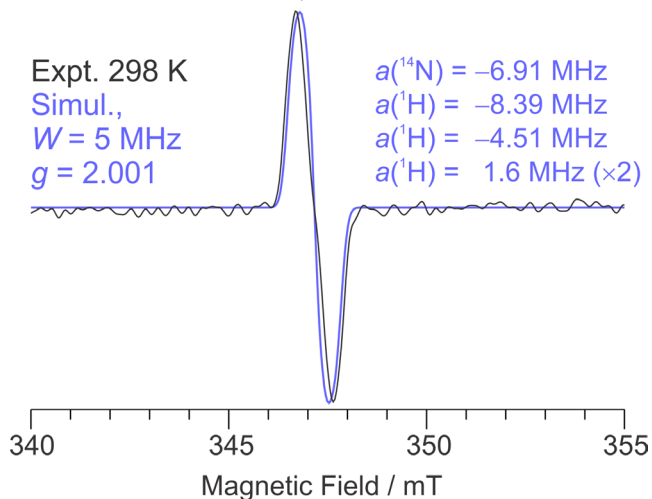


Figure 3. Room temperature X-band EPR spectrum (black trace) of **2** (4.9 mM in toluene; 9.72515 GHz; field modulation amplitude 4.0 G) with simulation (lavender trace). The simulation parameters are based on DFT calculations that provided isotropic hyperfine coupling constants for the ¹⁴N and ¹H nuclei in **2'-opt** (see Table S3; only the largest magnitude couplings are included). It is possible to simulate the experimental spectrum absent any hyperfine coupling, but with a broader linewidth (13 MHz, Gaussian, hwhm).

We also calculated the EPR parameters for **2'** and **2'-opt**; specifically, the *g* tensor and hyperfine coupling tensors for ¹⁴N and ¹H (Table S3). The values for **2'** and **2'-opt** are essentially identical, and only those of **2'-opt** will be discussed in detail. For comparison, these parameters were calculated also for PINO• (see SI for complete computational details). In all cases, the calculated *g* tensors were very close to the free electron value with anisotropy in the range of that observed experimentally. More importantly, the nitroxyl ¹⁴N hyperfine coupling calculated for **2'-opt** is reduced from that for PINO•, while coupling to the four H atoms of the aryl ring is increased relative to that for PINO•.⁷² As a consequence of the reduced |*A*(¹⁴N)| value and increased |*A*(¹H)| values, the EPR signal of **2** appears as a singlet, rather than the resolved triplet of PINO• and other related nitroxyl radicals.² The nature of the delocalization within the phthalimide fragment can also be seen by inspecting the relevant molecular orbital (91α in **2'-opt**), which is shown in Figure 4.

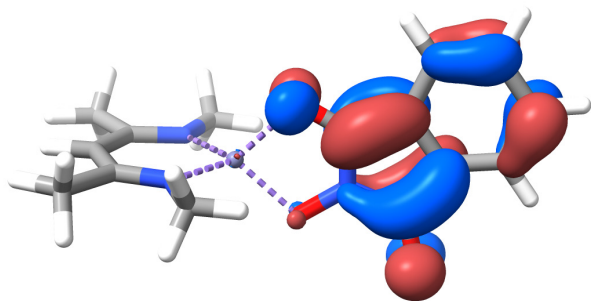


Figure 4. Isosurface (± 0.04 au) of the SOMO (91α) in **2'-opt**.

Intriguingly, the hyperfine coupling to ^{67}Zn is calculated to be non-zero (ranging from 1.5 – 2.0 MHz, depending on model). This value is too small to generate satellite peaks, in contrast to the spectrum observed for the closely-related Mg complex, $[\text{MeLMg}(\text{OCPH}_2)(\text{DMAP})]$.⁷³ Nonetheless, this prediction inspired us to use the results of Rieger to estimate what such a species would yield in terms of spin population on Zn (Table S6).^{74,75} In this regard, our extrapolation of Rieger's method corresponds to $<0.1\%$ of a spin, demonstrating that **2** is definitively a Zn(II) coordination complex.

In summary, we have structurally characterized the first example of a *N*-oxy-phthalimide complex featuring radical character within its phthalimide ligand, definitively establishing the redox activity of this ligand. Our EPR spectroscopic studies reveal a $S = 1/2$ delocalized organic radical with a smaller $|A(^{14}\text{N})|$ hyperfine coupling relative to typical nitroxyl radicals. These data are somewhat inconsistent with the solid-state metrical parameters of the reduced *N*-oxy-phthalimide fragment, which suggest that the radical is localized on a carbonyl group. Nonetheless, these structural and spectroscopic insights should facilitate further development of *N*-(acyloxy)phthalimide decarboxylation in organic synthesis. This work also expands the range of structurally-characterized redox-active ligands.

ASSOCIATED CONTENT

Supporting Information. Experimental procedures, crystallographic details, and spectral data for **1** and **2**, DFT procedures and output tables, along with further discussion of hyperfine coupling (PDF). This material is available free of charge via the Internet at <http://pubs.acs.org>

AUTHOR INFORMATION

Corresponding Author

* hayton@chem.ucsb.edu

Notes

The authors declare no competing financial interest.

ACKNOWLEDGMENT

This work was supported by the National Science Foundation (CHE 2055063). NMR spectra were collected on instruments supported by an NIH Shared Instrumentation Grant (1S100D012077-01A1). We thank Richard J. Jodts (Northwestern University, Evanston, IL) and especially Dr. Andrew Ozarowski (National High Magnetic Field Laboratory, Tallahassee, FL) for assistance with the use of ORCA software.

REFERENCES

1. Recupero, F.; Punta, C., Free Radical Functionalization of Organic Compounds Catalyzed by *N*-Hydroxyphthalimide. *Chem. Rev.* **2007**, *107*, 3800-3842.
2. Coseri, S., Phthalimide-*N*-oxyl (PINO) Radical, a Powerful Catalytic Agent: Its Generation and Versatility Towards Various Organic Substrates. *Catal. Rev.* **2009**, *51*, 218-292.
3. Melone, L.; Punta, C., Metal-free aerobic oxidations mediated by *N*-hydroxyphthalimide. A concise review. *Beilstein J. Org. Chem.* **2013**, *9*, 1296-1310.
4. Nutting, J. E.; Rafiee, M.; Stahl, S. S., Tetramethylpiperidine *N*-Oxyl (TEMPO), Phthalimide *N*-Oxyl (PINO), and Related *N*-Oxyl Species: Electrochemical Properties and Their Use in Electrocatalytic Reactions. *Chem. Rev.* **2018**, *118*, 4834-4885.
5. Murarka, S., *N*-(Aclyoxy)phthalimides as Redox-Active Esters in Cross-Coupling Reactions. *Adv. Synth. Catal.* **2018**, *360*, 1735-1753.
6. Luo, J.; Zhang, J., Aerobic Oxidation of Olefins and Lignin Model Compounds Using Photogenerated Phthalimide-*N*-oxyl Radical. *J. Org. Chem.* **2016**, *81*, 9131-9137.
7. Ishii, Y.; Iwahama, T.; Sakaguchi, S.; Nakayama, K.; Nishiyama, Y., Alkane Oxidation with Molecular Oxygen Using a New Efficient Catalytic System: *N*-Hydroxyphthalimide (NHPI) Combined with $\text{Co}(\text{acac})_n$ ($n = 2$ or 3). *J. Org. Chem.* **1996**, *61*, 4520-4526.
8. Gunchenko, P. A.; Li, J.; Liu, B.; Chen, H.; Pashenko, A. E.; Bakhonsky, V. V.; Zhuk, T. S.; Fokin, A. A., Aerobic oxidations with *N*-hydroxyphthalimide in trifluoroacetic acid. *Mol. Catal.* **2018**, *447*, 72-79.
9. Liang, F.; Zhong, W.; Xiang, L.; Mao, L.; Xu, Q.; Kirk, S. R.; Yin, D., Synergistic hydrogen atom transfer with the active role of solvent: Preferred one-step aerobic oxidation of cyclohexane to adipic acid by *N*-hydroxyphthalimide. *J. Catal.* **2019**, *378*, 256-269.
10. Sawatari, N.; Yokota, T.; Sakaguchi, S.; Ishii, Y., Alkane Oxidation with Air Catalyzed by Lipophilic *N*-Hydroxyphthalimides without Any Solvent. *J. Org. Chem.* **2001**, *66*, 7889-7891.
11. Ishii, Y.; Kato, S.; Iwahama, T.; Sakaguchi, S., Hydroxylation of polycyclic alkanes with molecular oxygen catalyzed by *N*-hydroxyphthalimide (NHPI) combined with transition metal salts. *Tetrahedron Lett.* **1996**, *37*, 4993-4996.
12. Bag, R.; Sar, D.; Punniyamurthy, T., Copper(II)-Catalyzed Direct Dioxygenation of Alkenes with Air and *N*-Hydroxyphthalimide: Synthesis of β -Keto-*N*-alkoxyphthalimides. *Org. Lett.* **2015**, *17*, 2010-2013.
13. Xia, X.-F.; Gu, Z.; Liu, W.; Wang, H.; Xia, Y.; Gao, H.; Liu, X.; Liang, Y.-M., Metal-Free Three-Component Oxyazidation of Alkenes with Trimethylsilyl Azide and *N*-Hydroxyphthalimide. *J. Org. Chem.* **2015**, *80*, 290-295.
14. Coseri, S.; Mendenhall, G. D.; Ingold, K. U., Mechanisms of Reaction of Aminoxyl (Nitroxide), Iminoxyl, and Imidoxyl Radicals with Alkenes and Evidence that in the Presence of Lead Tetraacetate, *N*-Hydroxyphthalimide Reacts with Alkenes by Both Radical and Nonradical Mechanisms. *J. Org. Chem.* **2005**, *70*, 4629-4636.
15. Huang, L.; Zheng, S.-C.; Tan, B.; Liu, X.-Y., Metal-Free Direct 1,6- and 1,2-Difunctionalization Triggered by Radical Trifluoromethylation of Alkenes. *Org. Lett.* **2015**, *17*, 1589-1592.
16. Masui, M.; Ueshima, T.; Ozaki, S., *N*-hydroxyphthalimide as an effective mediator for the oxidation of alcohols by electrolysis. *J. Chem. Soc., Chem. Commun.* **1983**, 479-480.
17. Bae, J. M.; Lee, M. M.; Lee, S. A.; Lee, S. Y.; Bok, K. H.; Kim, J.; Kim, C., Nonheme iron complex-catalyzed efficient alcohol oxidation by *t*-BuOOH with *N*-hydroxyphthalimide (NHPI) as co-catalyst: Implication of high valent iron-oxo species. *Inorg. Chim. Acta* **2016**, *451*, 8-15.

18. Iwahama, T.; Sakaguchi, S.; Ishii, Y., Production of Hydrogen Peroxide via Aerobic Oxidation of Alcohols Catalyzed by *N*-Hydroxyphthalimide. *Org. Process Res. Dev.* **2000**, *4*, 94-97.
19. Iwahama, T.; Sakaguchi, S.; Nishiyama, Y.; Ishii, Y., Aerobic oxidation of alcohols to carbonyl compounds catalyzed by *N*-hydroxyphthalimide (NHPI) combined with Co(acac)₃. *Tetrahedron Lett.* **1995**, *36*, 6923-6926.
20. Yang, G.; Zhang, Q.; Miao, H.; Tong, X.; Xu, J., Selective Organocatalytic Oxygenation of Hydrocarbons by Dioxxygen Using Anthraquinones and *N*-Hydroxyphthalimide. *Org. Lett.* **2005**, *7*, 263-266.
21. Ishii, Y.; Nakayama, K.; Takeno, M.; Sakaguchi, S.; Iwahama, T.; Nishiyama, Y., Novel Catalysis by *N*-Hydroxyphthalimide in the Oxidation of Organic Substrates by Molecular Oxygen. *J. Org. Chem.* **1995**, *60*, 3934-3935.
22. Lee, J. M.; Park, E. J.; Cho, S. H.; Chang, S., Cu-Facilitated C–O Bond Formation Using *N*-Hydroxyphthalimide: Efficient and Selective Functionalization of Benzyl and Allylic C–H Bonds. *J. Am. Chem. Soc.* **2008**, *130*, 7824-7825.
23. Iwahama, T.; Syojyo, K.; Sakaguchi, S.; Ishii, Y., Direct Conversion of Cyclohexane into Adipic Acid with Molecular Oxygen Catalyzed by *N*-Hydroxyphthalimide Combined with Mn(acac)₂ and Co(OAc)₂. *Org. Process Res. Dev.* **1998**, *2*, 255-260.
24. Gaster, E.; Kozuch, S.; Pappo, D., Selective Aerobic Oxidation of Methylarenes to Benzaldehydes Catalyzed by *N*-Hydroxyphthalimide and Cobalt(II) Acetate in Hexafluoropropan-2-ol. *Angew. Chem. Int. Ed.* **2017**, *56*, 5912-5915.
25. Yoshino, Y.; Hayashi, Y.; Iwahama, T.; Sakaguchi, S.; Ishii, Y., Catalytic Oxidation of Alkylbenzenes with Molecular Oxygen under Normal Pressure and Temperature by *N*-Hydroxyphthalimide Combined with Co(OAc)₂. *J. Org. Chem.* **1997**, *62*, 6810-6813.
26. Tan, Z.; Zhu, J.; Yang, W., Conjugated copper(II) porphyrin polymer and *N*-hydroxyphthalimide as effective catalysts for selective oxidation of cyclohexylbenzene. *Cat. Commun.* **2017**, *94*, 60-64.
27. Wang, C.; Harms, K.; Meggers, E., Catalytic Asymmetric C–H Functionalization under Photoredox Conditions by Radical Translocation and Stereocontrolled Alkene Addition. *Angew. Chem. Int. Ed.* **2016**, *55*, 13495-13498.
28. Okada, K.; Okamoto, K.; Oda, M., A new and practical method of decarboxylation: photosensitized decarboxylation of *N*-acyloxyphthalimides via electron-transfer mechanism. *J. Am. Chem. Soc.* **1988**, *110*, 8736-8738.
29. Okada, K.; Okamoto, K.; Morita, N.; Okubo, K.; Oda, M., Photosensitized decarboxylative Michael addition through *N*-(acyloxy)phthalimides via an electron-transfer mechanism. *J. Am. Chem. Soc.* **1991**, *113*, 9401-9402.
30. Montesinos-Magraner, M.; Costantini, M.; Ramírez-Contreras, R.; Muratore, M. E.; Johansson, M. J.; Mendoza, A., General Cyclopropane Assembly by Enantioselective Transfer of a Redox-Active Carbene to Aliphatic Olefins. *Angew. Chem. Int. Ed.* **2019**, *58*, 5930-5935.
31. Wang, C.; Yu, Y.; Liu, W.-L.; Duan, W.-L., Site-Tunable Csp³–H Bonds Functionalization by Visible-Light-Induced Radical Translocation of *N*-Alkoxyphthalimides. *Org. Lett.* **2019**, *21*, 9147-9152.
32. Wang, C.; Guo, M.; Qi, R.; Shang, Q.; Liu, Q.; Wang, S.; Zhao, L.; Wang, R.; Xu, Z., Visible-Light-Driven, Copper-Catalyzed Decarboxylative C(sp³)-H Alkylation of Glycine and Peptides. *Angew. Chem. Int. Ed.* **2018**, *57*, 15841-15846.
33. Qin, T.; Cornella, J.; Li, C.; Malins, L. R.; Edwards, J. T.; Kawamura, S.; Maxwell, B. D.; Eastgate, M. D.; Baran, P. S., A general alkyl-alkyl cross-coupling enabled by redox-active esters and alkylzinc reagents. *Science* **2016**, *352*, 801-805.
34. Zhao, W.; Wurz, R. P.; Peters, J. C.; Fu, G. C., Photoinduced, Copper-Catalyzed Decarboxylative C–N Coupling to Generate Protected Amines: An Alternative to the Curtius Rearrangement. *J. Am. Chem. Soc.* **2017**, *139*, 12153-12156.
35. Jin, Y.; Yang, H.; Fu, H., Thiophenol-Catalyzed Visible-Light Photoredox Decarboxylative Couplings of *N*-(Acetoxy)phthalimides. *Org. Lett.* **2016**, *18*, 6400-6403.
36. Mao, R.; Balon, J.; Hu, X., Decarboxylative C(sp³)-O Cross-Coupling. *Angew. Chem. Int. Ed.* **2018**, *57*, 13624-13628.
37. Li, C.; Wang, J.; Barton, L. M.; Yu, S.; Tian, M.; Peters, D. S.; Kumar, M.; Yu, A. W.; Johnson, K. A.; Chatterjee, A. K.; Yan, M.; Baran, P. S., Decarboxylative borylation. *Science* **2017**, *356*, eaam7355.
38. Yu, Z.; Mendoza, A., Enantioselective Assembly of Congested Cyclopropanes using Redox-Active Aryldiazoacetates. *ACS Catal.* **2019**, *9*, 7870-7875.
39. Chowdhury, R.; Mendoza, A., *N*-Hydroxyphthalimidyl diazoacetate (NHPI-DA): a modular methylene linchpin for the C–H alkylation of indoles. *Chem. Commun.* **2021**, *57*, 4532-4535.
40. Cornella, J.; Edwards, J. T.; Qin, T.; Kawamura, S.; Wang, J.; Pan, C.-M.; Gianatassio, R.; Schmidt, M.; Eastgate, M. D.; Baran, P. S., Practical Ni-Catalyzed Aryl–Alkyl Cross-Coupling of Secondary Redox-Active Esters. *J. Am. Chem. Soc.* **2016**, *138*, 2174-2177.
41. Zhang, J.; Li, Y.; Zhang, F.; Hu, C.; Chen, Y., Generation of Alkoxy Radicals by Photoredox Catalysis Enables Selective C(sp³)-H Functionalization under Mild Reaction Conditions. *Angew. Chem. Int. Ed.* **2016**, *55*, 1872-1875.
42. Edwards, J. T.; Merchant, R. R.; McClymont, K. S.; Knouse, K. W.; Qin, T.; Malins, L. R.; Vokits, B.; Shaw, S. A.; Bao, D.-H.; Wei, F.-L.; Zhou, T.; Eastgate, M. D.; Baran, P. S., Decarboxylative alkenylation. *Nature* **2017**, *545*, 213-218.
43. Lackner, G. L.; Quasdorf, K. W.; Overman, L. E., Direct Construction of Quaternary Carbons from Tertiary Alcohols via Photoredox-Catalyzed Fragmentation of *tert*-Alkyl *N*-Phthalimidoyl Oxalates. *J. Am. Chem. Soc.* **2013**, *135*, 15342-15345.
44. Tao, D. J.; Slutskyy, Y.; Overman, L. E., Total Synthesis of (–)-Chromodorolide B. *J. Am. Chem. Soc.* **2016**, *138*, 2186-2189.
45. Deng, Y.; Nguyen, M. D.; Zou, Y.; Houk, K. N.; Smith, A. B., Generation of Dithianyl and Dioxolanyl Radicals Using Photoredox Catalysis: Application in the Total Synthesis of the Danshenspiroketallactones via Radical Relay Chemistry. *Org. Lett.* **2019**, *21*, 1708-1712.
46. Jakob, A.; Schmidt, H.; Walfort, B.; Rheinwald, G.; Frühauf, S.; Schulz, S.; Gessner, T.; Lang, H., Tri-*n*-Butyl-Phosphan-Silber(I)-Komplexe mit Carboxylat-, Troponolat- bzw. *N*-Hydroxyphthalimid-Teilstrukturen; Synthese und Verwendung als Spin-On-Precursoren. *Z. anorg. allg. Chem.* **2005**, *631*, 1079-1086.
47. DiFranco, S. A.; Maciulis, N. A.; Staples, R. J.; Batrice, R. J.; Odom, A. L., Evaluation of Donor and Steric Properties of Anionic Ligands on High Valent Transition Metals. *Inorg. Chem.* **2012**, *51*, 1187-1200.
48. Wang, F.; Yin, H.; Yue, C.; Cheng, S.; Hong, M., Syntheses, structural characterization, in vitro cytotoxicities and DNA-binding properties of triphenylantimony di(*N*-oxyphthalimide) and di(*N*-oxy succinimide) complexes. *J. Organomet. Chem.* **2013**, *738*, 35-40.
49. Kaim, W., Manifestations of Noninnocent Ligand Behavior. *Inorg. Chem.* **2011**, *50*, 9752-9765.
50. Lyaskovskyy, V.; de Bruin, B., Redox Non-Innocent Ligands: Versatile New Tools to Control Catalytic Reactions. *ACS Catal.* **2012**, *2*, 270-279.
51. Fritz, M.; Schneider, S., The Renaissance of Base Metal Catalysis Enabled by Functional Ligands. *Struct. Bond.* **2019**, *182*, 1-36.

52. van der Vlugt, J. I., Radical-Type Reactivity and Catalysis by Single-Electron Transfer to or from Redox-Active Ligands. *Chem. Eur. J.* **2019**, *25*, 2651-2662.
53. Khan, F. F.; Chowdhury, A. D.; Lahiri, G. K., Bond Activations Assisted by Redox Active Ligand Scaffolds. *Eur. J. Inorg. Chem.* **2020**, *2020*, 1138-1146.
54. Mondal, R.; Guin, A. K.; Chakraborty, G.; Paul, N. D., Metal-ligand cooperative approaches in homogeneous catalysis using transition metal complex catalysts of redox noninnocent ligands. *Org. Biomol. Chem.* **2022**, *20*, 296-328.
55. Bernauer, J.; Pölker, J.; Jacobi von Wangelin, A., Redox-active BIAN-based Diimine Ligands in Metal-Catalyzed Small Molecule Syntheses. *ChemCatChem* **2022**, *14*, e202101182.
56. Pashanova, K. L.; Poddel'sky, A. I.; Piskunov, A. V., Complexes of "late" transition metals of the 3d row based on functionalized o-iminobenzoquinone type ligands: Interrelation of molecular and electronic structure, magnetic behaviour. *Coord. Chem. Rev.* **2022**, *459*, 214399.
57. Chirik, P. J., Iron- and Cobalt-Catalyzed Alkene Hydrogenation: Catalysis with Both Redox-Active and Strong Field Ligands. *Acc. Chem. Res.* **2015**, *48*, 1687-1695.
58. Matson, E. M.; Opperwall, S. R.; Fanwick, P. E.; Bart, S. C., "Oxidative Addition" of Halogens to Uranium(IV) Bis(amidophenolate) Complexes. *Inorg. Chem.* **2013**, *52*, 7295-7304.
59. Anderson, N. H.; Odoh, S. O.; Yao, Y.; Williams, U. J.; Schaefer, B. A.; Kiernicki, J. J.; Lewis, A. J.; Goshert, M. D.; Fanwick, P. E.; Schelter, E. J.; Walensky, J. R.; Gagliardi, L.; Bart, S. C., Harnessing redox activity for the formation of uranium tris(imido) compounds. *Nature Chem.* **2014**, *6*, 919-926.
60. Cladis, D. P.; Kiernicki, J. J.; Fanwick, P. E.; Bart, S. C., Multi-electron reduction facilitated by a trianionic pyridine(diimine) ligand. *Chem. Commun.* **2013**, *49*, 4169-4171.
61. Kaim, W.; Schwederski, B., Non-innocent ligands in bioinorganic chemistry—An overview. *Coord. Chem. Rev.* **2010**, *254*, 1580-1588.
62. Scepaniak, J. J.; Wright, A. M.; Lewis, R. A.; Wu, G.; Hayton, T. W., Tuning the Reactivity of TEMPO by Coordination to a Lewis Acid: Isolation and Reactivity of $MCl_3(\eta^1\text{-TEMPO})$ ($M = \text{Fe, Al}$). *J. Am. Chem. Soc.* **2012**, *134*, 19350-19353.
63. Wright, A. M.; Page, J. S.; Scepaniak, J. J.; Wu, G.; Hayton, T. W., Divergent Reactivity of TEMPO with MBr_3 ($M = \text{B, Al}$). *Eur. J. Inorg. Chem.* **2013**, *2013*, 3817-3820.
64. Nguyen, T.-A. D.; Wright, A. M.; Page, J. S.; Wu, G.; Hayton, T. W., Oxidation of Alcohols and Activated Alkanes with Lewis Acid-Activated TEMPO. *Inorg. Chem.* **2014**, *53*, 11377-11387.
65. Bourget-Merle, L.; Lappert, M. F.; Severn, J. R., The Chemistry of β -Diketiminatometal Complexes. *Chem. Rev.* **2002**, *102*, 3031-3066.
66. Yin, H.; Yue, C.; Hong, M.; Cui, J.; Wu, Q.; Zhang, X., Synthesis, structural characterization and in vitro cytotoxicity of diorganotin (IV) diimido complexes. *Eur. J. Med. Chem.* **2012**, *58*, 533-542.
67. Krishnakumar, V.; Sivasubramanian, M.; Muthunatesan, S., Density functional theory study and vibrational analysis of FT-IR and FT-Raman spectra of *N*-hydroxyphthalimide. *J. Raman Spectrosc.* **2009**, *40*, 987-991.
68. Miao, F.-M.; Wang, J.-L.; Miao, X.-S., *N*-Hydroxyphthalimide. *Acta Crystallogr., Sec. C* **1995**, *51*, 712-713.
69. Weil, J. A.; Bolton, J. R., *Electron Paramagnetic Resonance: Elementary Theory and Practical Applications, Second Edition*. John Wiley & Sons, Inc.: Hoboken, New Jersey, 2006.
70. Neese, F. *ORCA - an ab initio, Density Functional and Semiempirical Program Package, Version 4.0*, Max Planck Institute for Chemical Energy Conversion, 2017.
71. Neese, F., The ORCA program system. *Wiley Interdisciplinary Reviews: Computational Molecular Science* **2012**, *2*, 73-78.
72. The hyperfine coupling to the β -diketiminato ligand in **2'** is calculated to be negligible, but likely contributes to the intrinsic linewidth.
73. Murphy, D. M.; McDyre, L. E.; Carter, E.; Stasch, A.; Jones, C., A CW-EPR, ENDOR and special TRIPLE resonance study of a novel magnesium ketyl radical. *Mag. Res. Chem.* **2011**, *49*, 159-163.
74. Rieger, P. H., Atomic Hyperfine-Coupling Parameters for the Transition Metals. *J. Mag. Res.* **1997**, *124*, 140-146.
75. An Excel® spreadsheet that calculates the hyperfine coupling constants for nd atoms/ions ($n = 3, 4, 5$) in Groups 3 through 12 following the equations and parameters provided by Rieger (Ref. 74) for the entire range of relevant electronic configurations is available from J. Telsler. Rieger's paper provides only a few examples of the somewhat tedious calculations required to determine $\langle r^3 \rangle_{nd}$, $\langle r^3 \rangle_{(n+1)p}$, and $\psi(0)_{(n+1)s}^2$ (which then give P_{nd} , $P_{(n+1)p}$, and $A_{(n+1)s}$, respectively in MHz), but now all elements/configurations are available through this spreadsheet.

SYNOPSIS TOC: Characterization of $[K(2.2.2\text{-cryptand})][^{\text{Me}}\text{LZn(OPth)}]$ ($^{\text{Me}}\text{L} = \{(2,6\text{-}i\text{Pr}_2\text{C}_6\text{H}_3)\text{NC}(\text{Me})\}_2\text{CH}$) via X-ray crystallography and EPR spectroscopy reveals the presence of an $S = 1/2$ radical on the phthalimide ligand.

